Progresses in Developing Micro-Multilayer Multifunctional Electrical Insulation (MMEI) System for High Voltage Applications

Euy-sik Eugene Shin

NASA Glenn Research Center/Universities Space Research Association (USRA), 21000 Brookpark Rd., MS 49-1 Cleveland, OH 44135, USA

Fax: +1-(216)- 977-7132 E-mail address: euy-sik.e.shin@nasa.gov

Abstract

Development of the novel patented high voltage insulation system, namely micro-multilayer multifunctional electrical insulation (MMEI) was continued particularly for the future hybrid or all electric aircraft applications. Initially, the concept and feasibility of the MMEI system were successfully demonstrated with its exceptionally high dielectric breakdown voltage via optimizing the multilayer structures of the Kapton® PI films and binder layers such as PFA in terms of individual film thickness and layer configuration. Overall, MMEI structures outperformed most of the state-of-the-art (SOA) polymer insulation materials or structures. Since then, further optimizations and improvement of the system were pursued with specific emphasis on multifunctionalities such as moisture blocking, partial discharge (PD) resistance, durability, etc. Efforts have been also continued to identify the controlling mechanisms for the major improvement in dielectric strength of the MMEI structures via 3-dimensional dielectric failure mode analysis. At the same time, significant progress has been made in scaling up the MMEI structures and assessing their commercial applicability and manufacturability by developing full-scale prototypes of electrical components, such as power cable and bus bar. Overall progresses on the MMEI development to date will be presented in this paper.

Keywords: Novel Electrical Insulation System, Multilayer, High Voltage, Multifunctionality, Lightweight

Declarations

Funding: This work was supported by NASA's Transformational Tools and Technology (TTT) program under Transformative Aeronautics Concept Program (TACP), Aeronautics Research Mission Directorate (ARMD).

Conflicts of interest/Competing interests: The author has no relevant financial or non-financial interests to disclose.

Availability of data and material: The datasets generated during and/or analyzed during the current study are available from the corresponding author on reasonable request

Code availability: Not applicable

Acknowledgments

The author would like to thank Dan Scheiman, Paula Heimann, Toni Kapucinski, Tim Ubienski, Rich Martin, and Bill Brown at NASA-Glenn Research Center (GRC) for technical supports, and industrial collaborators, W. L. GORE & ASSOCIATES, INC., Landenberg, PA and MERSEN, New Product Development, Rochester, NY for prototype development, and the Center for High Performance Power Electronics (CHPPE, Prof. Jin Wang), Ohio State University, Columbus, OH for PD testing support. Furthermore, Maricela Lizcano, GRC is acknowledged as a project lead and for reviewing this paper and the rest of project team for their supports. This work has been sponsored by NASA's Transformational Tools and Technology (TTT) Program under the Aeronautics Research Mission Directorate (ARMD).

1.0 Introduction

As stated in Ref. [1, 2], one of the main challenges in designing fully electric or hybrid-electric propulsion aircrafts was to meet the high power requirement and to reduce weight of subsystems and cables. Conventionally, this would require larger currents and thus larger conductors which would result in huge weight and volume increase even though heavy mechanical and pneumatic machineries would be removed. One solution to avoid the larger conductors for a reasonable weight management was to employ high voltage (HV) systems. But then, it would require much thicker insulation with any SOA system which would again result in significant weight gain. On top of that, current HV cable technologies mostly developed for sea-level to low altitude applications were not suitable for the high-altitude aircraft applications due to much higher susceptibility to corona partial discharge (PD). In addition, the system should also meet high frequency and high temperature requirements. Therefore, developing a lightweight but high voltage, high temperature, and corona resistant insulation system was critically needed. As a response to such critical demands, a new high voltage, lightweight, and multifunctional electrical insulation system, namely micro-multilayer multifunctional electrical insulation (MMEI) was discovered under the NASA's Convergent Aeronautics Solutions (CAS) program from June 2015 to September 2017. Since then, the MMEI technology was patented, Ref. [3], and has been further developed and improved, particularly for high dielectric strength. Multifunctionality was another major thrust for the MMEI development obviously for its structural concept and design ability. Important multifunctionalities needed for high voltage insulation systems in the electrified aircraft applications included PD resistance, electro-magnetic interference (EMI) shielding, moisture barrier, mechanical durability, thermal management or/and heat dissipation and so on. However, achieving the multifunctionality will require extensive and systematic material-design-process optimizations, not by just simply adding some functional materials. It is worth noting that the MMEI structures could eventually take all the advantages of the Kapton® materials such as lightest weight, excellent physical thermal and electric properties, excellent cut-through resistance and cold flow resistance, excellent radiation resistance, good outgassing characteristics while their disadvantages such as inflexibility - difficult to strip, moisture absorption, degradation by atomic oxygen, poor weatherability, susceptibility to wet-arc and dry-arc tracking from abrasions and cuts, limited flexibility, instability to ultraviolet radiation could be mitigated.

The specific objectives of this work under the current NASA project were (i) to maximize dielectric performance of the new MMEI structures via material-design-process optimizations at minimum thickness, (ii) to incorporate multifunctionalities as many as possible, and (iii) to demonstrate scale-up, manufacturability, and commercial applicability of MMEI system via prototype development.

2.0 Experimental

All of the commercial materials tested or used in MMEI development and optimizations are updated below, but MMEI fabrication methods and dielectric strength test standards and procedures used in this work were consistent with those described in Ref. [1, 2]. It should be noted that, however, most dielectric properties presented in this paper were tested under the alternating current (AC) at 60 Hz frequency, at room temperature and room humidity unless specifically stated otherwise. In addition, details of serial polishing and image processing employed for the 3-dimensioal (3-D) dielectric breakdown damage and failure mode analysis are described in this section.

The typical layup convention for the MMEI configurations used throughout this paper is, for example, [1*HN/1*PFA]n/1*HN where the asterisk mark indicated thickness in mils (1/1000 of inch or 0.0254 mm), the capital letters stands for name or type of material, the slash for next layer, and the subscripted numbers after bracket for the number of repeated layup sequence within the bracket. In certain configurations, → is used after the initial number and asterisk followed by another set of number and indicates changes in film thickness from the initial number to the next number when the layup sequence is repeated.

2.1 Materials

All of the SOA commercial insulation materials and other functional materials which were purchased from various vendors including CS Hyde Company, American Durafilm, and McMaster-Carr for this work are listed below:

- Thermalimide Kapton® bagging film (KBF) (Airtech), 1, 2, & 5 mil: Thermally stable film
- Kapton® Polyimide (PI) high temperature high dielectric strength films (DuPont)
  - HN, 0.3, 1, & 5 mil: a general, tough aromatic film used as the baseline PI
  - HN, 05 & 1 mil with a silicone adhesive, 1 & 1.5 mil, backed film
  - HPP-ST or FPC, 0.5 & 1 mil: with superior dimensional stability and adhesion

  - CRC or CR, 1 mil: Corona resistant nano-composite film
- Perfluoroalkoxy (PFA), 0.5, 1, 2, 5, 10, 20 mil: Semi-crystalline polymer as bond layer
- Polyethylene terephthalate (PET), 2 mil: Semi-crystalline polymer as bond layer
- Polyetheretherketone (PEEK), 0.5, 2, 5 mil: Semi-crystalline/bond layer or Moisture barrier
- Teflon® PTFE, 1, 2, 3, 5, 10, 15, 20, 40, 62.5 mil: Moisture barrier
- Flexible Electrical-Insulating Mica (FEIM), 4 mil: Corona PD barrier

For the purpose of comparison with MMEI structures, a commercial alternative multilayer candidate, CIRLEX® Kapton® HN laminate sheet, 10 mil and 20 mil thick, designated in this work as CK10 and CK20, respectively, developed by Fralock with the proprietary adhesiveless lamination process was also evaluated in this study.

2.2 Serial Polishing and Image Processing

Serial polishing and subsequent high resolution micrographing of the polished cross-sections were carried out by using the RoboMet.3D automated system (UES, Inc., Dayton, OH). The sample for the Robo-Met process was prepared by encapsulating test specimens with a mounting resin, usually a fluorescent epoxy, like the one for the typical metallurgical polishing. Since the system was capable of taking exceptionally high resolution micrographs, i.e., micrographs can be significantly magnified without losing damage zone (DZ) details during the post-image processes, multiple test specimens were mounted in one sample, thus, reduced the overall process time significantly. Fig. 1 illustrates the axial coordinate system for the Robo-Met sample containing multiple test specimens arranged against the direction of current flow during the dielectric strength testing. With the coordinate system, DZ evolution and failure path of every tested specimens were determined consistently. It should be also noted that polishing on the xz-plane perpendicular to the current or voltage direction presented better DZ view against layers, thus clearer damage propagation and failure paths through the layers while polishing on the xy-plane could capture the entire DZ contour easier. The automatic serial polishing was set to cover the entire DZs, typically up to 10 to 20 mm, by removing the smallest practical amount, ~ 50 - 100 µm, between cross-sections, and to take high resolution micrograph of ~ 1 gigabyte in file size at each cross-section. Since the original micrographs contained multiple cross-sectional images of all test specimens, they were further processed for more effective 3-D dielectric breakdown damage and failure mode analysis. The post-image analysis processes were mostly performed with the ImageJ software (Fiji, an open source image processing package, https://imagej.net/Fiji) which involved separation of cross-sectional images per specimen, transformation of the images to maintain consistency in shape, orientation, and magnification and thus to enhance DZ, and measurements of its dimensions.

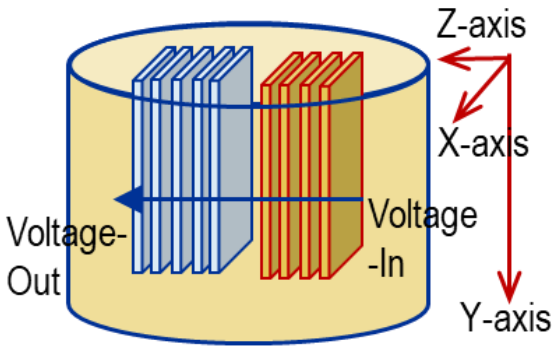

Fig. 1 Coordinate system for the encapsulated RoboMet sample for automatic serial polishing

3.0 Results and Discussion

3.1 Characterizations of the SOA insulation materials

In order to evaluate the potentials of the MMEI system more accurately and practically, extensive and systematic characterizations of the SOA insulation materials and structures were performed. Fig. 2 summarizes dielectric breakdown voltages (V_B) of various commercially available SOA insulation materials as a function of overall sample thickness tested in either oil or air. PTFE or PFA was available with a wide range of thickness while most Kapton® materials were available only up to 5 mils (0.127 mm). All data points were generated at GRC following the standardized test conditions, Ref. [1, 2]. It should be noted that the HN air data were somewhat deviated from the data presented by the manufacturer in the literature apparently due to different test conditions. In most cases, the best curve fitting for the V_B-*thickness (t)* relation roughly followed a logarithmic trendline regardless of material type or test medium. Interestingly enough, however, the changes in V_B by changing the test medium from oil to air were dependent on both material type and thickness. For PTFE, $V_{B,OIL}$ was greater than $V_{B,AIR}$ initially with thinner

thickness, but $V_{B,AIR}$ became equal to or greater than $V_{B,OIL}$ with increasing thickness having the transition at ~ 0.8 mm. PFA seemed to follow the same trend, but it was not certain since they were only tested up to 0.51 mm thickness. For PEEK, however, the transition occurred much sooner, at ~ 0.05 mm or thinner. In the case of Kapton® PI, both $V_{B,OIL}$ and $V_{B,AIR}$ were about same initially for thicknesses less than 1 mil (0.0254 mm), but $V_{B,AIR}$ was significantly lower than $V_{B,OIL}$ for 5 mil thick samples for both KBF and HN. This opposite behavior in $\Delta V_{B,\,AIR\text{-}to\text{-}OIL} - t$ relation between Kapton® PI materials and semi-crystalline bond-layer materials is clearly illustrated in Fig. 3. Overall, PFA showed the least changes.

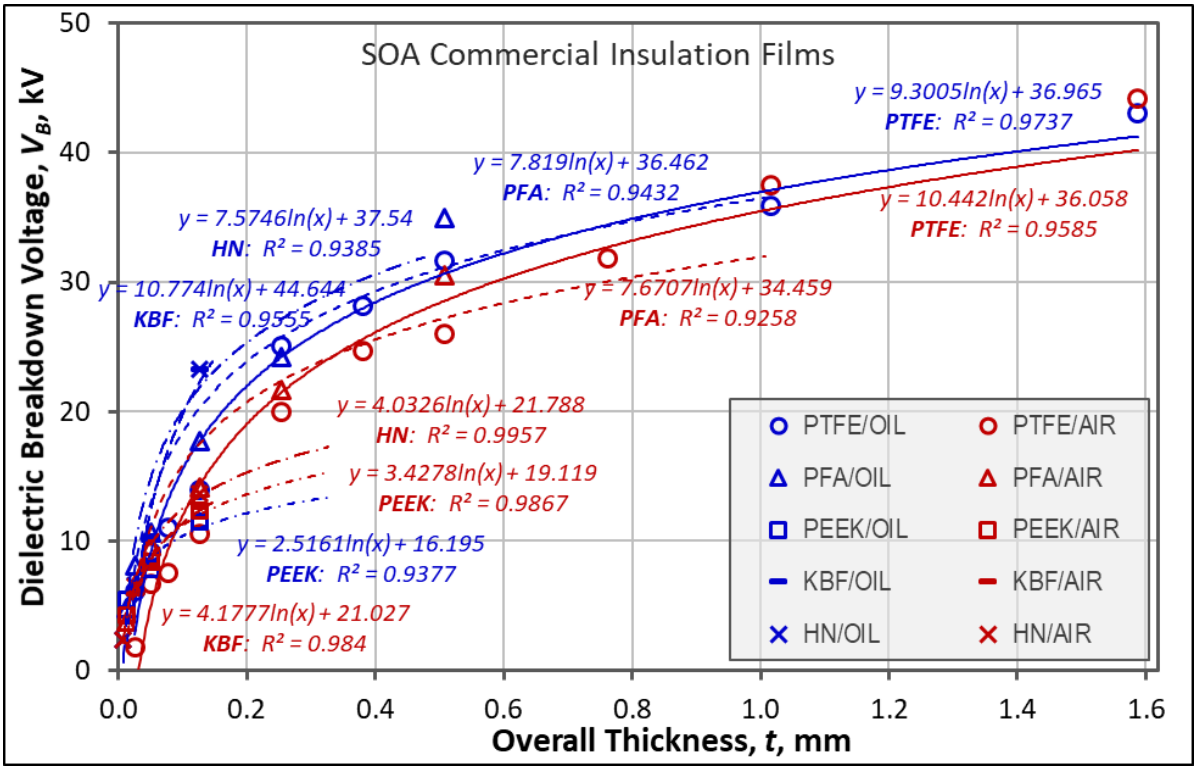

Fig. 2 V_B of various SOA commercial insulation materials as a function of thickness in either oil or air with the best-fit trendlines

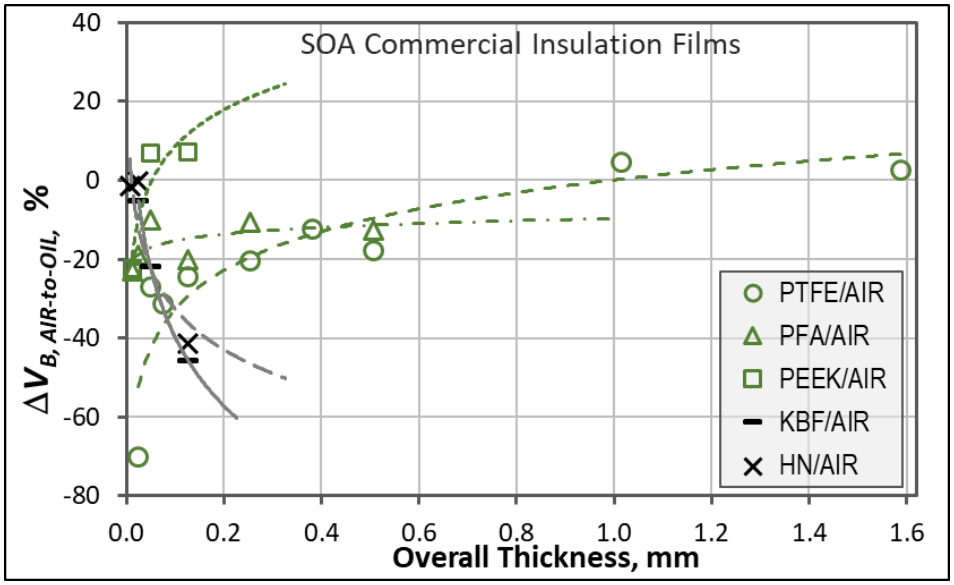

Fig. 3 $\Delta V_{B\,AIR\text{-}to\text{-}OIL}$ of the SOA insulation materials as a function of thickness

3.2 Status of MMEI Development

With the general dielectric performance of the SOA materials fully characterized, performance of the MMEI structures was assessed more accurately. V_B values of the newly improved or optimized MMEI structures to date in either oil or air are superimposed onto the V_B-t trendlines of the SOA insulation materials in Fig. 4. The Cirlex® laminates, CK10 and CK20, and the most well-known SOA aircraft insulation system, TKT (Ref. [4, 5]) were also included for direct comparison. Note that the TKT, 2*PTFE/5*HN/2*PTFE, tested in this work was not a commercial product but fabricated in the lab based on Ref. [4] by employing the same process used for MMEI structures. V_B of TKT was slightly lower than that of Kapton® materials but almost equal to that of PTFE. In addition, the drops in V_B when tested in air, mostly of the better-performing MMEI configurations, [1*HN/1*PFA]n/1*HN, are compared directly to other insulation materials. The designations of the MMEI structures listed in Fig. 4 were as follows:

- With the better-performing configurations, 17H0 for n = 3, 17H for n = 4, 17H1 for n = 5, 17H2 for n = 6, 17H3 for n = 8, 17H4 for n = 10
- BS12 or '12': 5*KBF/5*PFA/5*KBF
- 17X: 0.3*HN/$[1*PFA/1*HN]_{10}$/$[1*PFA/1*CR]_2$/2*PEEK/0.3*HN
- 17X1: 0.3*HN/$[1*PFA/1*HN]_{10}$/2*PEEK/4*FEIM
- KT1: $[1*HN/1.5*Si]_4$/1*HN and KT2: $[0.5*HN/1*Si]_8$/1*HN

Both 17X and 17X1 configurations were developed as candidates for the full-scale component prototypes involving additional multifunctionalities such as moisture barrier and corona PD resistance which will be discussed later. Overall, the MMEI structures, particularly the better-performing configurations, showed the highest V_B values regardless of sample thickness, typically around 70 – 90% higher than the projected values of the base Kapton® HN material, which would result in significant reductions in insulation thickness or weight. Other MMEI structures such as PI-PET MMEI ($[1*KBF/2*PET]_4$/1*KBF configuration only) or PI-Si MMEI (KT1 and KT2) did not perform as well, but they were developed for lower temperature applications or applications requiring high flexibility, respectively. In the case of PI-Si MMEI, they were physically bonded with silicone adhesive (using a non-hardening pressure sensitive silicone) at room temperature instead of fuse-bonding or cure, thus extremely flexible and the adhesive was rated for 400 - 500°F (204 – 260°C) use.

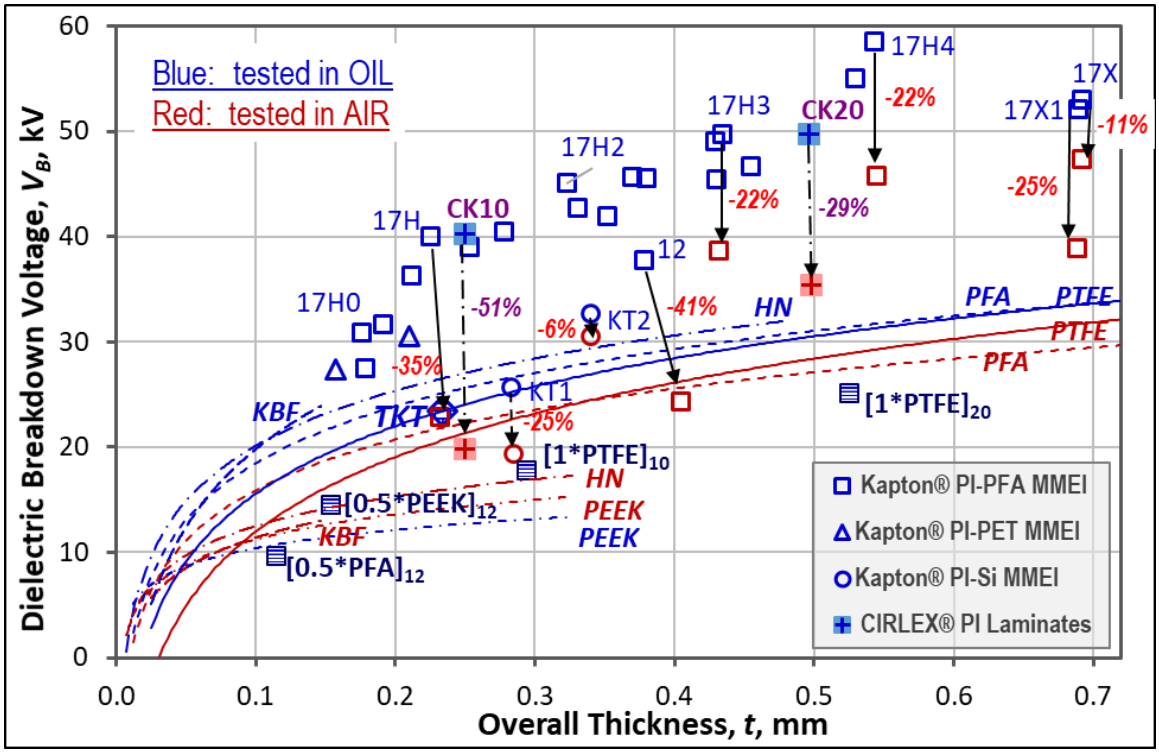

Fig. 4 Overall dielectric performance of various MMEI structures to date compared to the SOA commercial insulation materials and structures including TKT and Cirlex® laminates

The Cirlex® laminates, CK10 and CK20, also performed very well, almost comparable to the better-performing MMEIs. Although they were made with a proprietary process, it was suggested that a thermal lamination process was applied on multiple layers of Kapton® HN films without any adhesives. Based on the concept, similar laminates were fabricated with other fuse-bondable insulation materials such as PEEK, PTFE, and PFA by a simple compression-molding process in order to ascertain whether the interfaces played any role in improving V_B compared to their homogeneous bulk materials. However, all of those laminates including $[0.5*PFA]_{12}$, $[0.5*PEEK]_{12}$, $[1*PTFE]_{10}$, and $[1*PTFE]_{20}$ performed rather poorly as shown in Fig. 4. Since interlayer bonding integrity of all of those laminates and Cirlex® laminates was confirmed to be good without any defects, the role of interfaces on V_B must be material dependent. In any case, efforts will be continued to identify potential mechanisms of the improved dielectric performance of the Cirlex® laminated structures.

In the case of the V_B drop when tested in air rather than oil, $\Delta V_{B,\ AIR\text{-}\ to\text{-}OIL}$, the order of change from the smallest to the largest per material type was PFA, PTFE, PEEK < PI-Si MMEI < PI-PFA MMEI < Cirlex® laminates < Kapton® PI films. Note that the drop was greater for the Cirlex® laminates than most MMEI structures at the comparable overall sample thicknesses. It was clear that the drop of the better-performing MMEI was smaller than that of other MMEI, e.g., BS12 or 12. Overall, the improved and optimized Kapton® PI-PFA MMEI structures outperformed all of the tested SOA insulation materials or other commercial structures in both V_B and $\Delta V_{B,\ AIR\text{-}\ to\text{-}OIL}$. Interestingly enough, the large $\Delta V_{B,\ AIR\text{-}\ to\text{-}OIL}$ of the Kapton® PI films might be related with the changes in the pre-breakdown damage evolution, such as cavitation, microcracking or cracking. When tested in oil, these features were clearly visible and grew to a large DZ prior to the ultimate dielectric breakdown, but none of the DZ features mentioned were present when tested in air. The DZ was considered as an electric energy absorber, i.e., more energy must be required to form the DZ and subsequently higher breakdown voltage in oil or much less energy or lower V_B without such DZ in air. On the other hand, PFA, PTFE, or PEEK within the sample thicknesses tested showed no visible pre-breakdown DZ features nor were there noticeable changes in overall failure mode whether tested in oil or air.

Since the initial attempt for the systematic parametric analyses of the MMEI structures at the beginning, Ref. [1], the efforts were continued to validate the effects of the critical parameters that controlled their dielectric strength with more batches of the improved and optimized MMEI structures. As summarized in Fig. 5, the additional data points consistently followed the original overall trends and behavior, i.e., validated the effects of various structural parameters on dielectric performance. The results of the parametric analyses are used as the practical design guidelines for further optimizations as well as design of future MMEI structures per specific application requirements.

Fig. 6 summarizes the average leakage current (LC) at three different applied voltages for various SOA insulation materials including Cirlex® laminates and MMEI structures as a function of sample thickness as tested in either oil or air. The LC was well-defined as a pass-through current under the applied voltage, more prominently under AC, that a dielectric can sustain without leading to runaway currents as a result of dielectric breakdown. It is related to the dielectric material not being a perfect insulator and having some non-zero conductivity, thus, it can be relatable to PD potentials. The LC was monitored and determined during dielectric breakdown testing as another dielectric performance parameter of insulation materials. A typical LC limit was 0.5 mA. Clearly, the LC was affected by both material and thickness or structure as well as test medium, oil vs. air. For PTFE, LC in air was higher than that in oil initially at thinner samples but showed opposite trend with increasing thickness regardless of the applied voltage, but the sample thicknesses for the transition were ~ 0.07, 0.13, and 0.8 mm for 2, 5, and 15 kV, respectively. PFA and PEEK seemed to follow the similar trend and transitions. Kapton® PI also followed similar trends, but LC in air was much higher than that in oil initially compared to other materials. Now, by comparing all other insulation materials or structures, the overall LC from the largest to the smallest per material type was: (i) in oil, laminates of PEEK, PTFE, PFA > TKT > Cirlex® PI laminates ≥ MMEI structures ≅ SOA materials, but (ii) in air, Cirlex® PI laminates >> MMEI structures > SOA materials regardless of the applied voltage level. Note that LC of Cirlex® PI laminates was always higher than that of MMEIs regardless of the applied voltage or test environment (OIL vs. AIR), especially for 10 mil (0.254 mm) thick sample.

Additionally, based on the nature of LC, it could be used to assess thermal stability of insulation materials. As an example, LC of 5*PFA increased considerably after being exposed at 350 °C even for a short time, but no visible changes from any of Kapton® PI films including 0.3*HN, 0.5*FPC, 1*KBF, or 5*KBF after such thermal exposure. This behavior was consistent with the changes in V_B reported previously, Ref. [1]. That is, the Kapton® PI films did not undergo any thermal-induced molecular structural changes or degradation, thus no changes in LC or have better thermal stability than PFA.

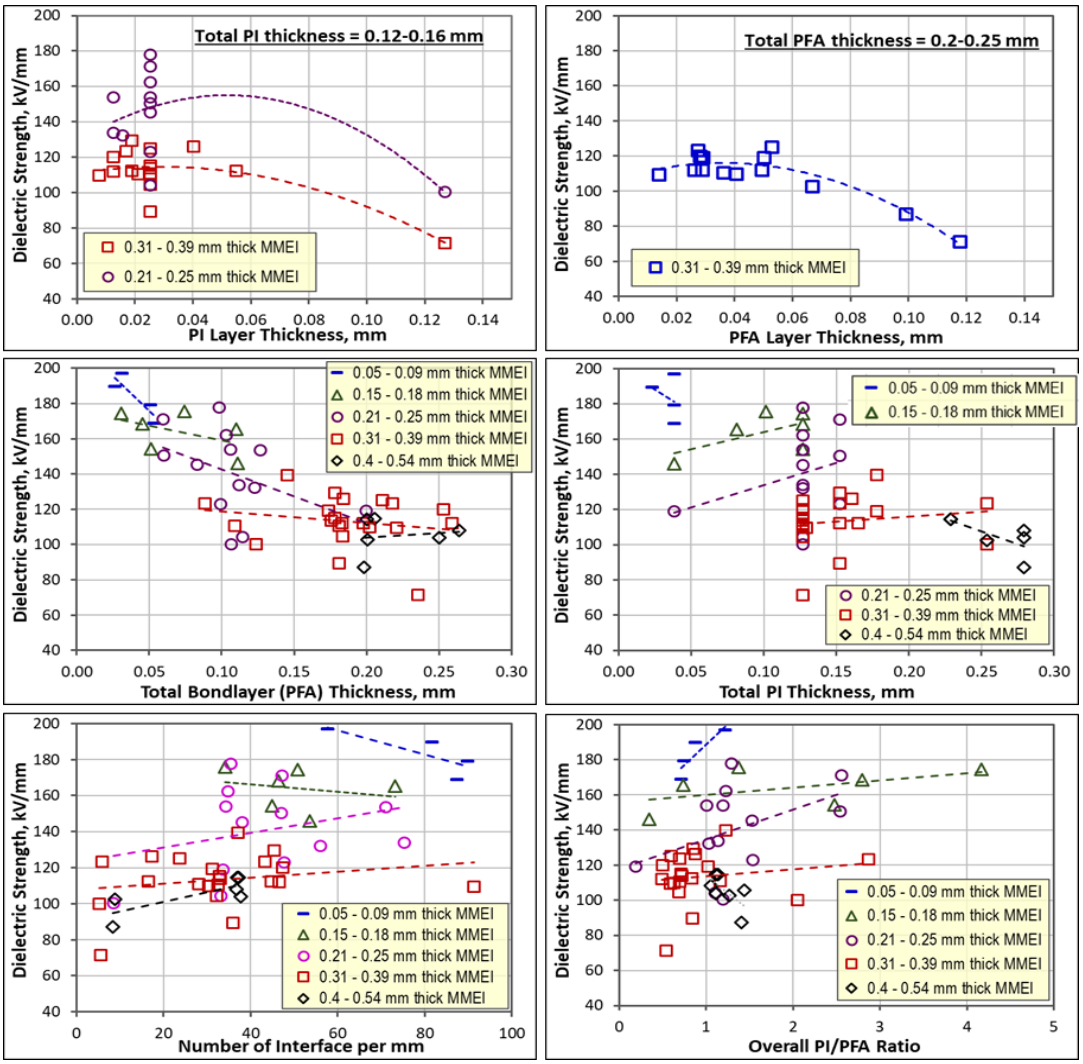

Fig. 5 Updated MMEI parametric analyses

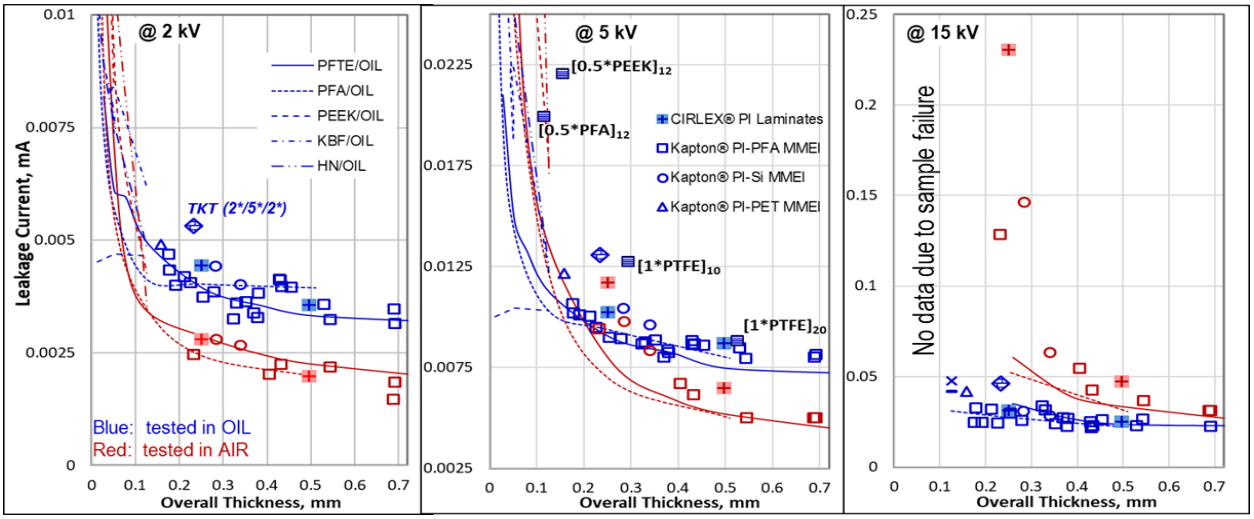

Fig. 6 Leakage current of various insulation materials and structures as a function of overall sample thickness at various applied voltages

The effects of current type, AC vs DC, on V_B of the SOA insulation materials and MMEI structures were assessed with a few representative samples in oil. As summarized in Fig. 7, $V_{B,DC}$ was significantly higher than $V_{B,AC}$ for all tested sample types. As indicated by the percent increases in the plot, PFA unexpectedly outperformed Kapton® PI films, HN and KBF, or Cirlex® laminate, CK10, under DC at the comparable sample thicknesses. The % increase in V_B of CK10 was about same as the Kapton® PI films regardless of its laminated structure or thickness. However, all tested MMEI structures showed potentially much higher increases in $V_{B,DC}$ than the typical SOA insulation materials or Cirlex® PI laminates since none of them failed up to the maximum applicable voltage, 84 kV, of the test system. By directly comparing 17H and CK10 at the similar overall thickness, it was certain that MMEI structure outperformed Cirlex® laminate under DC, more than under AC. As clearly represented in micrographs in Fig. 7, all Kapton® PI materials and MMEI samples showed no pre-failure damages, such as cavitation, micro-crack, or crack, under DC even in oil medium similar to what happened in air. As discussed earlier, the changes in the pre-breakdown damage modes of the Kapton® materials might be associated with the lesser increase in V_B than PFA.

Based on the test results to date, the overall comparison between the Cirlex® laminates and the MMEIs was attempted. While the Cirlex® laminates showed comparable V_B under certain test conditions and may have better mechanical strength than MMEIs, the best-performing MMEIs seemed to outperform the Cirlex® laminates, demonstrating higher V_B in general, lower LC, better durability, lower moisture absorption, easier multifunctionalities, more flexible design, processability, and applicability via various methods. Additionally, there is a potentially lower cost via the reduced usage of the high priced Kapton® materials (< 60%) as well as the lower processing cost.

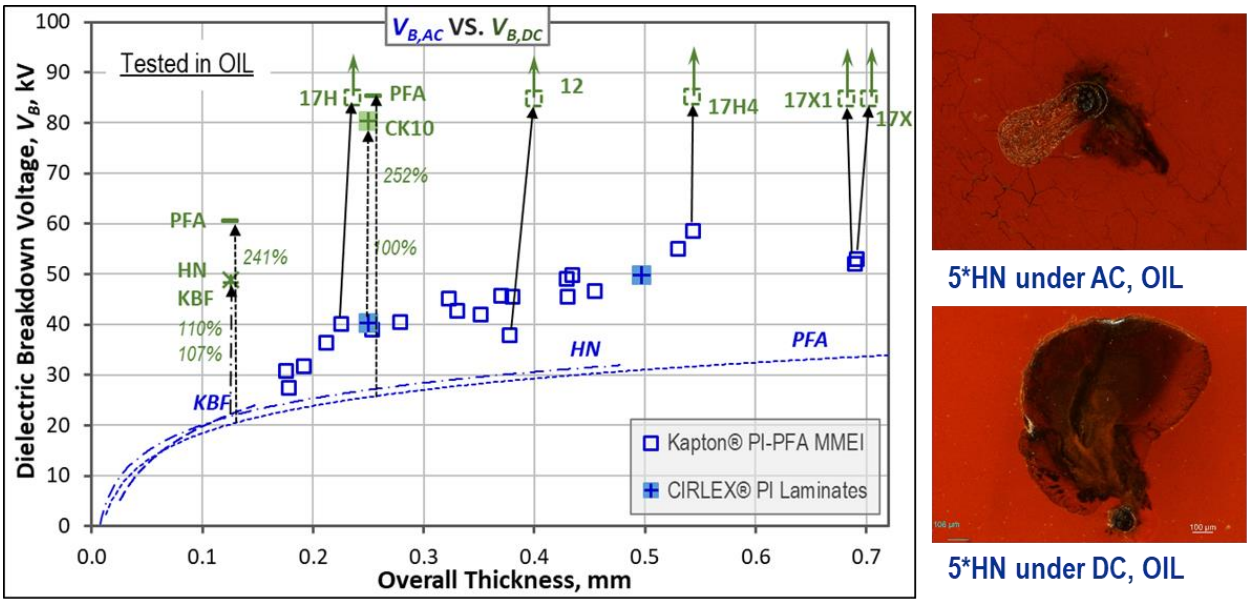

Fig. 7 $\Delta V_{B\ DC\text{-}to\text{-}AC}$ of various insulation materials and structures, and the typical pre-breakdown DZ mode changes in 5*HN

As a part of MMEI development, another key effort was initiated to characterize partial discharge (PD) behavior including corona PD of various MMEI structures as well as the SOA insulation materials and structures in collaboration with the center for high performance power electronics (CHPPE), Ohio State University (OSU). The PD inception voltage and extinction voltage (PDIV/PDEV) were systematically determined as functions of pressure from 1 atm down to 100 torr (at 48,000 ft altitude), DC vs. AC, frequency, pulse width modulation (PWM) voltage, and possibly temperature or other service environmental conditions. Both flat coupon samples with various thicknesses and the full-scale component prototypes to be discussed later were to be tested. Based on the preliminary test results, it was observed that (i) PDIV of polymer insulation was thickness dependent, but not clear whether the MMEI system followed the same trend or performed differently, (ii) For PDIV, most semi-crystalline polymers performed equal to or better than most Kapton® PI materials, and (iii) as expected, PDIV of all samples dropped significantly at the lower pressure of 100 torr and its rate increase with thickness also slowed considerably. It is anticipated that PDIV/PDEV will dictate down-selection of insulation system for the high altitude applications. In addition, as a part of identifying mechanisms for improved V_B of MMEI structures, capacitance of the SOA insulations and several MMEI structures was measured as a function of frequency at the CHPPE. In general, they were small, less than ~4 nF, but showing some trends as a function of frequency and sample thickness and possible differences in

trend between the SOA insulation materials and MMEI structures. The efforts are being continued for more comprehensive and systematic test results.

3.3 MMEI Mechanisms

As presumed previously, Ref. [1, 2], the potential mechanisms responsible for the improved MMEI performance could be any one or combinations of the following list or other unknown mechanisms: (i) molecular rearrangement-induced changes in capacitance or conductance, (ii) formation of more torturous path for electron move by multilayered structures, (iii) less or smaller void formation within thinner layers formed by heat fuse-bonding resulting in less PD, and (iv) increased space charge formation/storage capacity at interfaces resulting in lower voltage potentials. In any case, they need to be validated experimentally in order to further optimize MMEI configurations and thus to maximize its performance. The experimental efforts being made to date included 3-dimensional (3D) dielectric breakdown failure mode analysis and Pulsed Electro-Acoustic (PEA) analysis. Furthermore, another effort has been made to predict dielectric performance of the MMEI structures via electromagnetic and electro-thermo-mechanical modeling in terms of the material-structural parameters as well as their service exposure conditions for the high voltage materials and structures. The initial results of the baseline study were published in Ref. [6] but more elaborated modeling of the MMEI system is under way. While determining how space charges move through bulk materials or interfaces and mapping the charge distribution, etc. and affect MMEI performance by the PEA technique required more systematic and in-depth analyses, significant progresses have been made for the 3D damage and failure mode analysis. As described in the experimental section, the analysis was performed by the Robo-Met automatic serial polishing and micro-graphing processes. At first, 9 different specimens were investigated including CK20, BS12, 17H4, 17X, both tested in oil and air and TKT tested in oil all under AC, Fig. 8. In this trial, a total of 95 high resolution cross-sections separated by 50 -100 µm spacing were obtained, thus covered the overall DZ length of about 7.4 mm along the y-axis. The accurate spacing distances between the neighboring cross-sections were automatically tabulated during the serial polishing and used to determine DZ dimensions later. However, the serial polishing process of the rest of the sample was to continue since, for a couple of specimens, their DZs were not fully revealed.

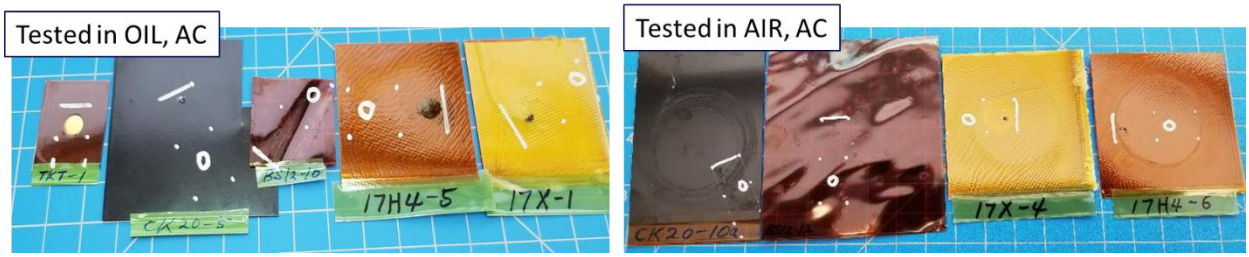

Fig. 8 Various tested specimens initially prepared for 3-D failure mode analyses (Note that failure sites, thus where to cut and mount, were clearly marked)

Fig. 9 shows the sequence of the representative cross-sections of 0.545 mm thick 17H4 MMEI sample consisting of 21 layers which failed under dielectric breakdown test in air. The sample was one of the best performing MMEI structures with V_B = 44.1 kV in air. The magnification of the micrographs was indicated by the scale bar at the lower right corner, but for the detailed analysis, much higher magnifications were used without losing resolution. The direction of current/voltage flow was always from right to left through the thickness of the sample. The typical damage mode observed from this sample included in-pane cracking and charring-disintegration of Kapton® HN layers; interlayer debonding and propagation; cavitation in PFA layer if thicker than ~ 2 mil (0.05 mm); melting and disintegration of PFA layer, mostly within DZ. Note that thickness of PFA layer varied noticeably in most layers which could be considered as a weakness of the structure. Efforts will be made to mitigate the issue by improving and optimizing the process conditions. Based on the damage mode sequence, it appeared that the local voltage was intensified at the interlayer interfaces and released through repetitive sequence of interlayer debonding and propagation followed by thru-layer-perforation process, resulting in a lengthier, more torturous failure path. From the analysis, it was also determined that planar dimensions of the DZ perpendicular to the current/voltage direction were 5.5 mm in x-axis and 5 mm along y-axis since the zone was spanned from the cross-section #8 to #80. Also shown in the cross-sections are where the high voltage break-in's (by blue arrows) and out (by the purple arrow) or debond propagations (by the pink arrows). With these, the distance between the voltage-in and -out, L, was measured. The other MMEI structure 17X which was selected for the component prototypes also displayed very similar damage and failure modes as the 17H4 when failed under dielectric breakdown test in air, i.e., in-plane cracking and charring-disintegration of Kapton® layers of HN and CR; interlayer debonding and propagation; cavitation in PEEK and PFA

layers if thicker than ~ 2 mil; melting and disintegration of PFA and PEEK layers. The 17X consisting of 27 layers with overall thickness of 0.692 mm and V_B of 47.9 kV in air formed a DZ of 4.5 mm in x-axis and 3 mm in y-axis.

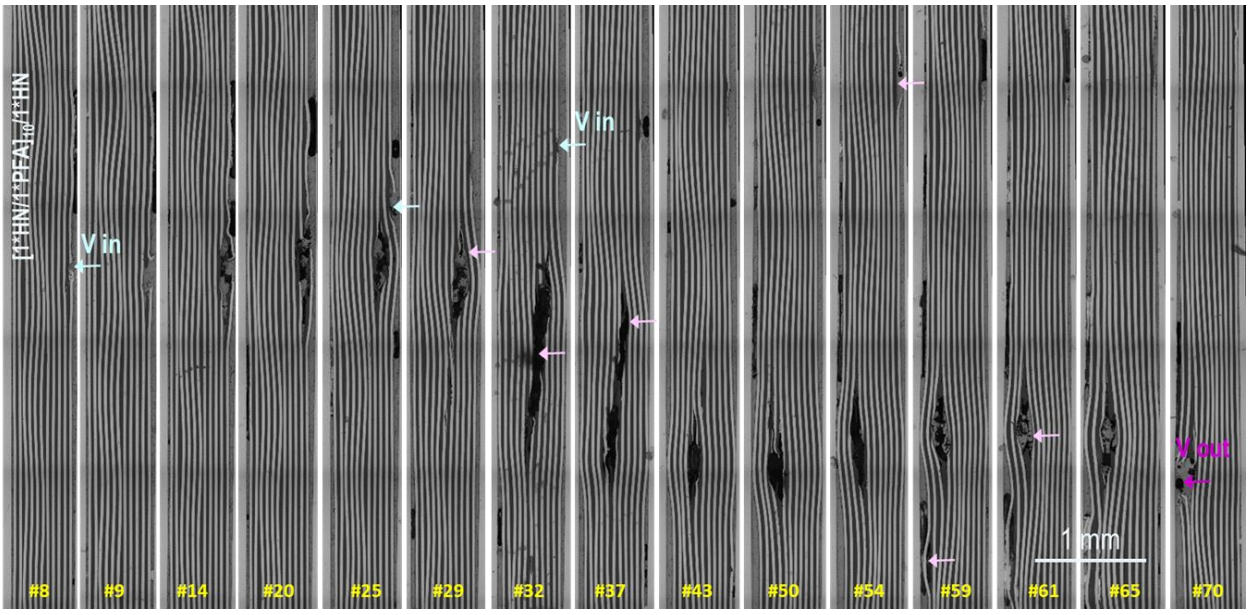

Fig. 9 Sequence of representative cross-sectional micrographs showing typical damage and failure modes of 17H4 MMEI after failed in air (Note the sequencial number of each cross-section at the bottom)

The damage and failure mode sequence of the 17H4 sample in oil (V_B = 58.3 kV) looked slightly different than those failed in air but progressed by a similar lengthier, more torturous failure path, Fig. 10, involving micro-cavitation and microcracking on the outermost Kapton® HN layers; cavitation and charring-disintegration of internal Kapton® HN layers; interlayer debonding and propagation; melting- disintegration of PFA layers. Note the two different scale bars for x- and z-axis, respectively, for asymmetric scale. Overall, its DZ was much larger, 12 mm in x-axis and > 8 mm in y-axis (the DZ extended beyond the last cross-section #96). Similarly, the 17X in oil (V_B = 53.8 kV) was damaged and failed by micro-cavitation & microcracking on the outermost Kapton® HN layers; cavitation and charring-disintegration of internal Kapton® layers of HN and CR; interlayer debonding and propagation; melting-disintegration of PFA and PEEK layers. The final DZ dimensions were _10.9 mm in x-axis and >7.5 mm in y-axis.

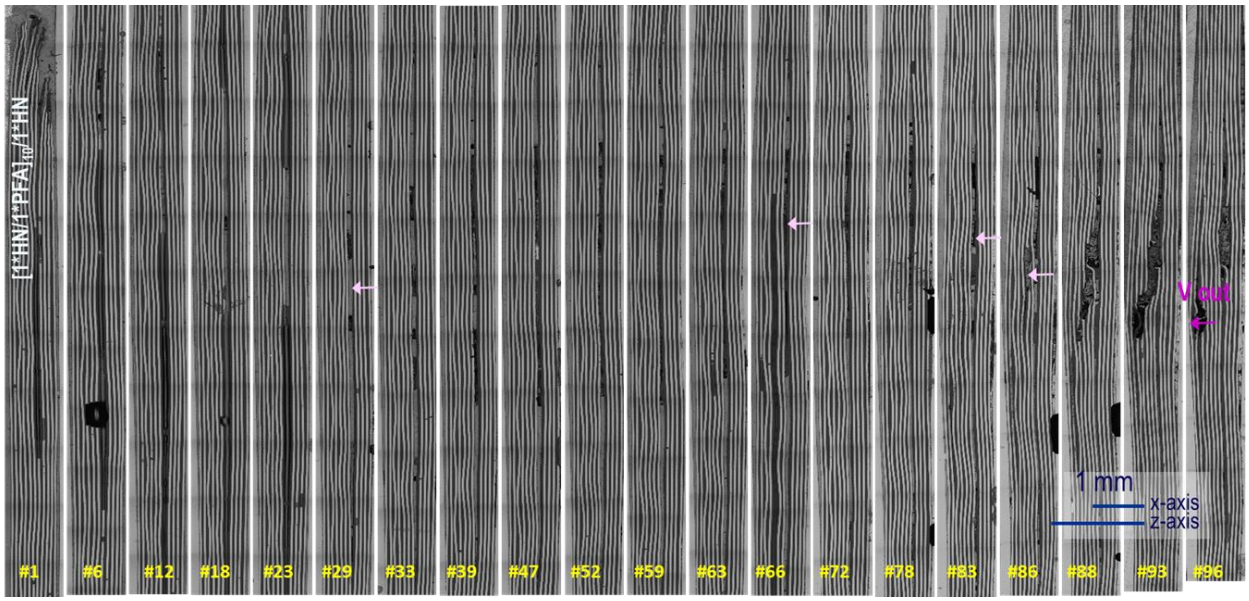

Fig. 10 Same as Fig. 9 but after failed in oil

In the case of the BS12 MMEI consisting of 3 thicker layers of KBF and PFA with overall thickness of 0.4 mm which resulted in lower V_B of 24.6 kV in air, its damage and failure modes involved in-pane cracking and charring-disintegration of KBF layers; extensive cavitation, melting, and disintegration of PFA layer. However, their overall failure path was rather simpler and straightforward via cavitation, cracking and thru-layer-perforation, Fig. 11. That is, high voltage perforated right through the layers even though it caused several large cavitation spreading around, mostly in the PFA layer. Its overall DZ was narrower and concentrated, 3.3 mm in x-axis and 1.2 mm in y-axis.

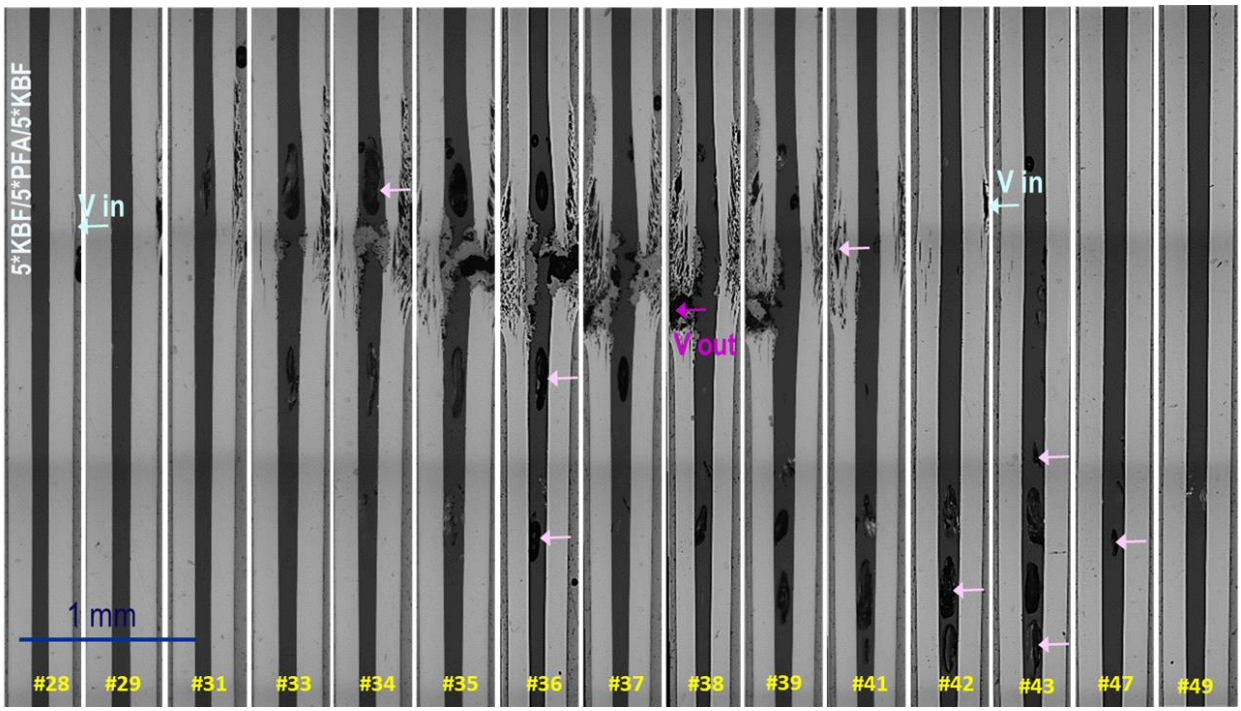

Fig. 11 Same as Fig. 9 but for BS12 MMEI

Fig. 12 shows the sequence of damage and failure mode of the BS12 sample when tested in oil (V_B = 45.8 kV). For this sample, the full DZ was not entirely covered with the initial serial polishing, thus voltage break-in or out points could not be located. In any case, its damage modes included micro-cavitation, microcracking, charring-disintegration of KBF layers; excessive cavitation, melting-disintegration of PFA layer. It seemed that its dielectric failure was simply propagated via cracking and cavitation. Its DZ dimensions with the available cross-sections were 5.9 mm in x-axis and 5 mm in y-axis but could be larger. A similar damage and failure mode was also observed from the 3-layer TKT sample in oil (V_B = 22.3 kV), i.e., cavitation, mostly in-plane cracking, charring-disintegration of Kapton® HN layer; interlayer debonding and propagation; cavitation, cracking, melting-disintegration of PTFE layers. Its overall DZ dimensions were 1.9 mm in x-axis and 3.5 mm in y-axis.

Both samples of the CK20 Cirlex® laminate tested in air and oil were analyzed for the 3-D damage and failure path. However, the sample failed in air did not reveal any major damage or failure modes except a few surface cracks and localized charring. It might be the case that the initial serial polishing did not cover the entire damage zone and failure path, particularly sites for the voltage break-in or -out, thus it will be attempted again when the follow-up serial polishing is completed. On the other hand, damage and failure modes of the sample tested in oil (V_B = 53.8 kV) are displayed in Fig. 13 and involved mostly micro-cracks, in-plane cracks, cavitation, and charring-disintegration of Kapton® layers. Surprisingly, its DZ was somewhat confined within 3.9 mm in x-axis and 3.5 mm in y-axis. Its dielectric failure progressed via cracking, in-plane splitting but not necessarily along the interlayer interfaces probably due to stronger interface bonding, and charring-disintegration which can be considered as an intermediate degree of failure path between 17H4 and BS12 in terms of complexity.

In summary, for most samples, dielectric failure in oil involved more in-plane damage modes with a larger DZ while the failure in air involved more localized and thru-thickness damage propagation probably due to different local electric field distribution. Typical damage/failure modes were (i) cavitation, cracking (either micro or macro and either in-plane or thru-thickness), and charring in the Kapton® layers, (ii) cavitation and melting in the semi-crystalline bond-layers; and (iii) interlayer debonding and propagation, till they were locally or completely disintegrated.

Dimensions of microcrack were ~ 30 μm in both depth and width as marked in green arrows in Fig. 12, and mostly appeared on outermost layers, particularly the side of voltage-out. It is worth noting again that the DZ type strongly dependent on layer thickness, e.g., (i) profuse and larger cavitation in thicker PFA layers in BS12, but no cavitation in thinner PFA layers of 17X or 17H4 (ii) cracking in internal Kapton® layers in oil, only if layer thickness > 1 mil. This suggested that decreasing layer thickness less than 1 mil effectively suppressed damage evolution or possibly decrease PD with smaller defects/voids within layers.

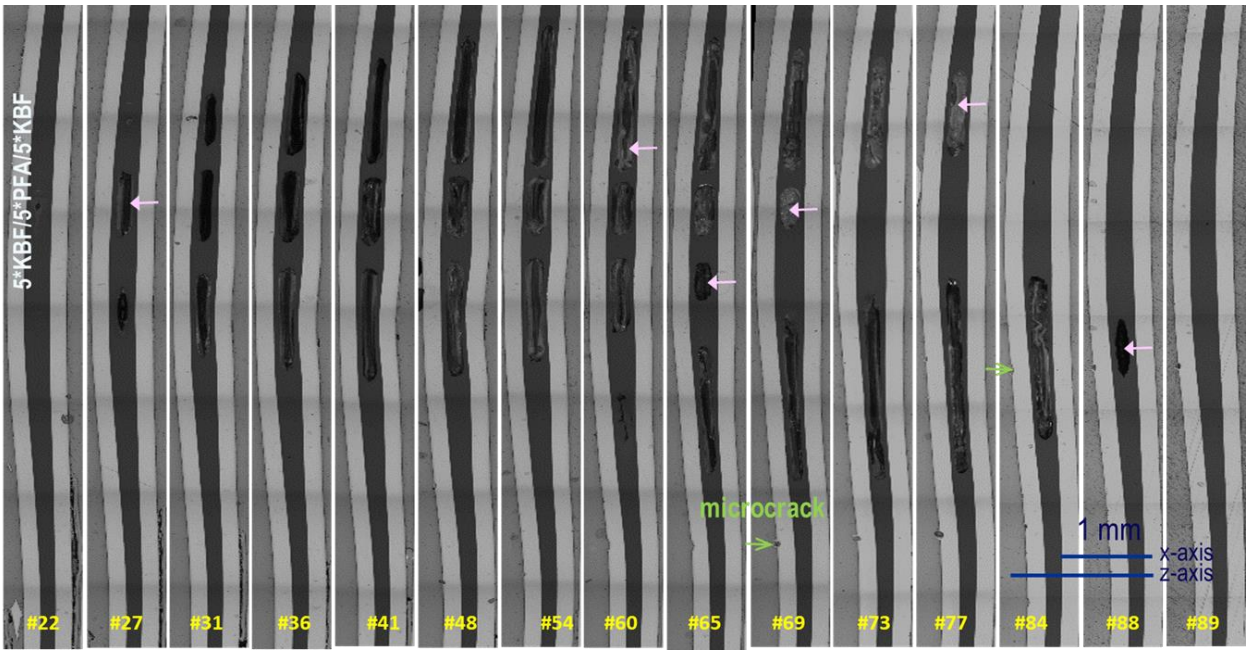

Fig. 12 Same as Fig. 11 but after failed in oil

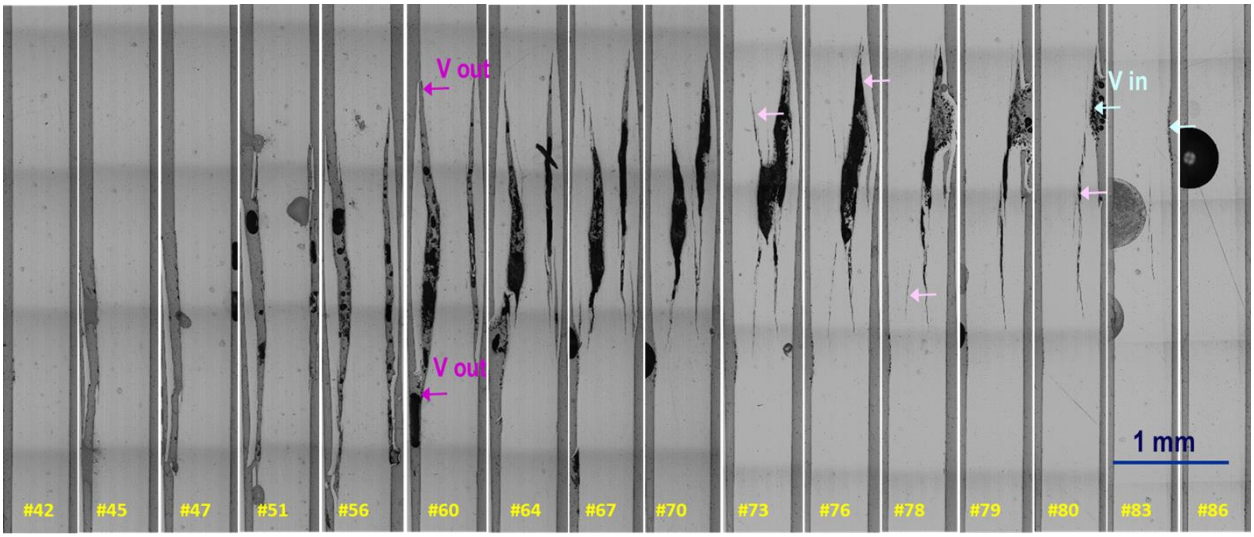

Fig. 13 Same as Fig. 12 but for CK20 laminate

Based on the quantitative DZ analysis, the MMEI structure - DZ – V_B relations were ascertained as summarized in Fig. 14 and Fig. 15. The dimensions of the overall DZ, either in x-axis or in y-axis or by the distance between V_{in} and V_{out} positions, L, was more proportionally related with V_B than overall thickness for the samples tested in oil except CK20, but much smaller changes when tested in air. It is clear that much larger DZ in the better-performing MMEI structures resulted in higher V_B. However, in the case of CK20 Cirlex® laminate tested in oil, its DZ was much smaller than other MMEIs. This suggested that potential mechanisms of the improved V_B might be different from those of the MMEIs. Additionally, the intensities of DZ were also quantified by the opening thickness and number of the interlayer

debond, Fig. 15. As expected, both 17X and 17H4 MMEI structures were associated with much larger number and wider openings of the interlayer debond than other structures tested. It is certain that interlayer debonding and propagation were the unique damage/failure mode in the high performance MMEI structures, and more extensive when tested in oil. However, it was also of interest to note that the opening thickness of CK20 debond was comparably wide which supported the DZ – V_B relations to some extent. Overall, this 3-D damage mode analysis confirmed that the size of DZ was directly proportional to V_B in general. Furthermore, the 3-D failure mode analyses confirmed two of the suggested mechanisms responsible for MMEI performance, that is 'formation of more torturous path for HV current flow from multilayered structures', and the effects of individual layer thickness from the parametric analyses as another mechanism, i.e., 'damage formation/evolution was effectively suppressed with decreasing the individual layer thickness', along with another suggested mechanism, 'less chance of defects/voids existing in thinner film or smaller defects/voids in thinner film, thus less partial discharge'.

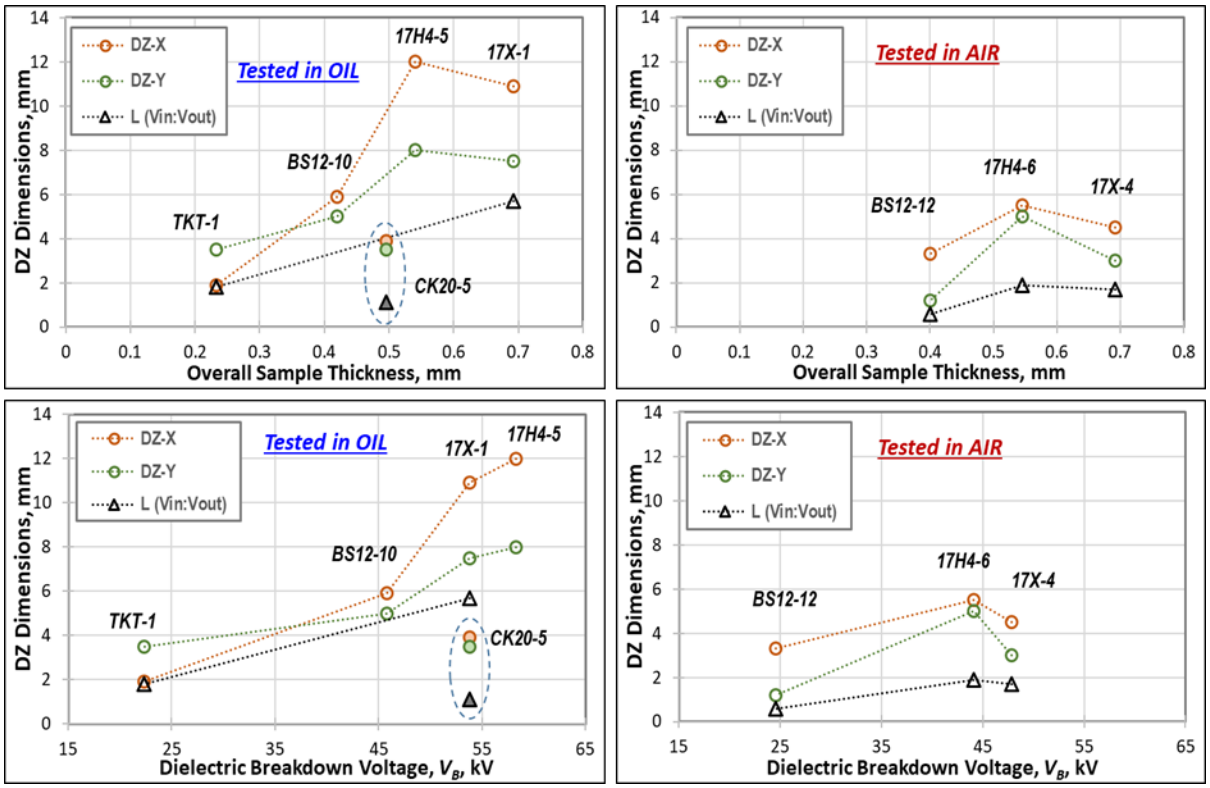

Fig. 14 Quantification of DZ of various insulation systems in terms of overall sample thickness (top) and V_B (bottom)

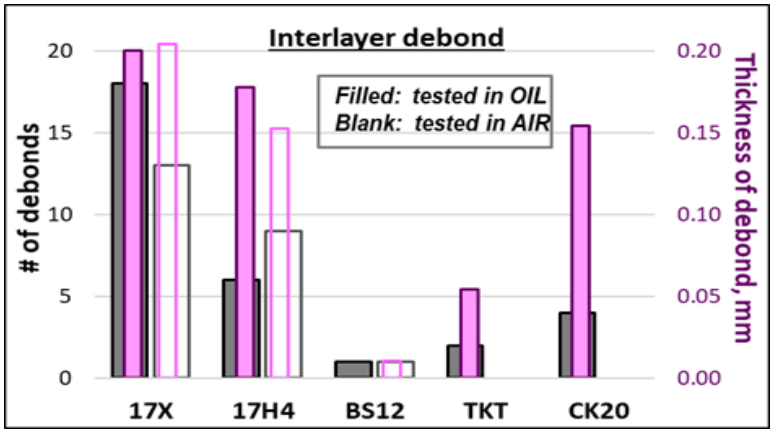

Fig. 15 Quantification of debond DZ of various insulation systems

3.4 Scale-up and Commercial Applicability

The efforts to assess the scalability and commercial applicability of the MMEI system were continued via developing full-scale prototypes of representative electrical components for the future electric aircrafts, such as bus bar and power cable. As reported earlier, Ref. [2], development of bus bar prototypes was collaborated with the MERSEN, New Product Development, Rochester, NY while the power cable prototype was with the W. L. GORE & ASSOCIATES, INC., Landenberg, PA. The basic approach employed in the work was to design and manufacture two prototypes per component type, one by the collaborator using their best insulation as the commercial SOA system and the other by GRC using one of the optimized MMEI system, and thus, to achieve more practical and meaningful assessment. Obviously, everything else except the insulation such as conductor design and mounting mechanisms was fixed for both prototypes. For the GRC prototypes, based on the improved dielectric and potential PD performance as well as the moisture barrier function, the 17X MMEI was down-selected at potentially reduced weight and volume.

For the bus bar prototype, the base design of the 1-m long, 3 phase, high voltage and high frequency capable prototypes was described in Ref. [2] in details. To date, the prototype by the MERSEN was completed and evaluated with the basic standard tests as also detailed in Ref. [2]. In the case of the GRC prototype, the specific application details via one-step lamination autoclave process were optimized and finalized, particularly temperature control along the entire length of the 1-m long prototype. Note that the first 0.3*HN layer in the 17X configuration should be replaced with additional PFA layers when they were installed onto the metal conductors, but the optimum thickness of the PFA layer was not optimized yet. Thus, the combined effects of PFA layer thickness and fuse-bonding temperature on bonding integrity between MMEI and metal conductors were investigated. Four sets of four peel strength samples with various numbers of PFA layers were assembled directly onto the 83-mm wide × 1-m long conductor blank at various locations via the autoclave process. The same overall sample thickness of ~0.254 mm was maintained for all. At the same time, their temperatures were monitored respectively. The sample sets including (i) P1-1, 2, 3, 4: 1*PFA/2*KBF/[1*→2×1*PFA/2*KBF]$_2$, (ii) P2-1, 2, 3, 4: [1*PFA]$_2$/2*KBF/[1*PFA/2*KBF]$_2$, (iii) P3-1, 2, 3, 4: [1*PFA]$_3$/2*KBF/[1*PFA/2*KBF]$_2$, and (iv) P5-1, 2, 3, 4: 5*PFA/2*KBF/1*PFA/2*KBF were distributed from the one end of the conductor to the other end, respectively. Dimensions of the samples were 5/8"(15.9 mm) wide × 4" (102 mm) long with 1.5" (38 mm) long crack initiator by 0.3*HN film and two samples were fit within the width of the conductor. The fuse-bonding temperatures of the sample sets varied from 655°F/346°C to 672°F/356°C, thus, the ΔT_{max} among the sample sets was about 17°F/10°C. After the fuse-bonding of the sample assemblies in autoclave, the conductor bar was directly mounted to the Instron test frame and the samples were pulled one by one at 0.5 inch/min cross-head speed at room temperature, room humidity. Fig. 16 summarizes the overall test results. The PFA bonding integrity in terms of both peel strength (ultimate load to failure) and toughness (area under load-displacement curve to failure) was good for the thickness range from 1 mil/0.025 mm up to 3 mils/0.076 mm but decreased significantly at the thickness of 5 mil or 0.125 mm. Consequently, a 2 mil/0.051 mm thick PFA layer was selected, i.e., aluminum (Al) conductor/1*PFA/[1*PFA/1*HN]$_{10}$/[1*PFA/1*CR]$_2$/2*PEEK/0.3*HN as the final insulation system for the prototypes. Similarly, good bonding integrity was maintained between 655°F/346°C and 667°F/353°C of the fuse-bonding temperature until sharp decreases above the latter temperature. Thus, the range was used as a target fuse-bonding temperature in optimizing the autoclave process for the prototype fabrication provided that the temperature should never exceed 667°C/353°C on any part of the 1-m long bus bar.

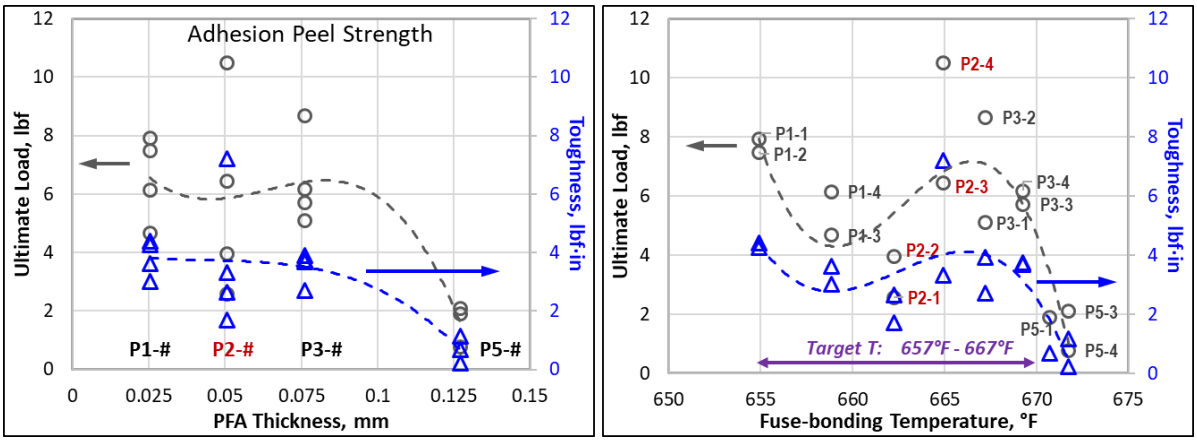

Fig. 16 Optimization of bus bar prototype fabrication with 17X MMEI in terms of PFA thickness against metal conductor (left) as well as fusebonding temperature (right)

Based on the above test results, various attempts were made to reduce the maximum temperature gradient, ΔT_{max}, along the 1-m long bus bar prototype during the autoclave process and identified an optimum temperature-vacuum-pressure-time profile. At the same time, the overall quality of the prototype insulation in terms of defect-free insulation, seamless edge finishes or smooth surfaces was improved via autoclave material-design-process optimizations. Fig. 17 displays photographs of a representative unit of the successful bus bar conductors with the MMEI insulation to date. The full-size GRC prototype will be assembled with three conductor units and evaluated by the basic standard tests at the MERSEN, but eventually both prototypes will be evaluated for more comprehensive and systematic PD performance under the aforementioned synergistic service environments in collaboration with the CHPPE-OSU.

Fig. 17 Photographs of a completed conductor with 17X MMEI for GRC bus bar prototype showing high quality finish

The prototype development for the power cable was also under way. As described in Ref. [2], a flat pod cable consisting of six identical conductors, which were arranged horizontally and capable of carrying 0.25 MW at 15 kV or higher (rated to 40 kV), was designed by the GORE. The GORE prototype employed its proprietary PTFE-PTFE composite insulation and a corona resistant PTFE jacket, rated to -80 ºC ~ >260 ºC, was completed and being evaluated at GRC and CHPPE-OSU. For the GRC prototype, similar efforts as the bus bar prototype development described above are being made to manufacture 1-m long cable sections via a batch process of one-step autoclave lamination with the 17X MMEI system.

4.0 Summary and Conclusions

The newly developed MMEI system was further optimized and improved. Key findings included:

- MMEI structures outperformed most of the SOA insulation materials in terms of $V_{B,AC}$ or $V_{B,DC}$
- $[1*HN/1*PFA]_N/1*HN$ configurations performed best, and the highest improvement to date was 91% with N=10 (or ~98% reduction in insulation thickness) compared to the Kapton® HN, and outperformed Cirlex® PI laminates in terms of V_B, $DV_{B,\ AIR\text{-}to\text{-}OIL}$, or leakage current (LC).
- In general, adding functional layers caused negative impact on the overall V_B of MMEI and it was not only material dependent but also structure dependent, thus, more systematic and careful design and optimizations required to incorporate multifunctionalities into MMEI.
- Potential Mechanisms responsible for MMEI performance were suggested and some have been validated experimentally via 3-D dielectric breakdown damage and failure mode analyses.

Significant progress was made in scaling up, assessing commercial applicability, and manufacturing full-scale prototypes of MMEI system:

- The down-selected MMEI for the initial GRC prototypes of HV HP power cable and bus bar with its superior V_B and anticipated multifunctionalities was further optimized for PFA-conductor bonding integrity; Al conductor/1*PFA/$[1*PFA/1*HN]_{10}$/$[1*PFA/1*CR]_2$/2*PEEK/0.3*HN, and will be compared to the SOA commercial systems.

5.0 Future Work Plan

The following tasks are planned to continue for development and improvement of the MMEI system:

- Material-design-process optimizations, especially for additional multifunctionalities, such as EMI shielding, thermal management, or mechanicals, and development of new/modified constituent materials with improved performance
- Experimental validation of potential mechanisms on performance enhancement of MMEI structures via 3-D damage and failure mode analyses, PEA space charge behavior characterizations, and electro-thermo-mechanical modeling, etc.
- Continuation of scale up, prototype developments, and commercialization
- More sophisticated performance evaluations of the MMEI structures/prototypes including synergistic durability assessment
- Thermal-mechanical-physical performance characterizations including interlayer adhesion integrity

References

1. Shin, E. E., Scheiman, D. A., Lizcano, M.: Lightweight, durable, and multifunctional electrical insulation material systems for high voltage applications. Proceedings of the 1st AIAA/IEEE Electric Aircraft Technologies Symposium (EATS) (2018). https://doi.org/10.2514/6.2018-5013
2. Shin, E. Eugene: Development of high voltage micro-multilayer multifunctional electrical insulation (MMEI) system. Proceedings of the AIAA/IEEE Electric Aircraft Technologies Symposium (EATS) (2019). https://doi.org/10.2514/6.2019-4511
3. Shin, E. E.; High performance multilayer insulation composite for high voltage applications. United States Patent (U.S. Pat.) No. 10,546,666, January 28, 2020
4. Cinibulk, W.: Aircraft electrical wire - Wire manufacturers perspective. Tyco Electronics (Raychem). https://www.mitrecaasd.org/atsrac/FAA_PI-Engineer_Workshop/2001/aircraft_electrical_wire.pdf. Accessed 5 May 2021
5. Paterson, A.: Aircraft electrical wire types associated with aircraft electric fires. http://www.vision.net.au/~apaterson/aviation/wire_types.htm. Last Updated: 22 July 2012. Accessed 30 March 2015
6. Naghipour, P., Woodworth, A., Shin, E., Lizcano, M., Nguyen, V., and Zhupanska, O.: Modeling of electro-magneto-thermo-mechanical interactions in high voltage materials and structures for electric propulsion. NASA/TM-20210011828, NASA Glenn Research Center, June 2021